A Study of Thermal Parameters and Interdendritic Feeding in Lost Foam Casting

Qiming Chen and C. Ravindran

(Submitted 13 September 1999; in revised form 7 April 2000)

Thermal parameter-based criterion functions are of great practical importance to predict dispersed microporosity in castings. Using an experimental approach, the present study is a pioneering application of the thermal parameter-based criterion functions to predict the microporosity formation in lost foam casting (LFC) of A356 alloy. A series of plate castings with controlled hydrogen content were made with various thermal conditions by varying the dimensions of feeders and in gate design. Extensive analysis of the thermal parameters shows that changing the gate and feeder design modifies the distribution of the thermal parameters; furthermore, it influences the distribution of microporosity along the central line of the plate castings. The thermal parameters and criterion functions based on Darcy's law show consistency, thus supporting the interdendritic feeding mechanism of microporosity formation. The criterion functions such as *Niyama, LCC,* and *KCL* can be used to predict microporosity formation during solidification of LFC, depending on the hydrogen content in the casting. The limitation of the interdendritic feeding mechanism and the effect of hydrogen on the gas pore formation are also discussed.

Keywords alloy A356, heat treating, interdendritic feeding, lost foam casting, microporosity, thermal parameters

1. Introduction

Castability, high strength-to-weight ratio, and corrosion resistance have placed A356 aluminum alloy castings in an indispensable position in the aircraft and automobile industry. However, the susceptibility of the A356 alloy to the formation of microporosity is attributed to a relatively wide freezing range, good thermal conductivity, and high latent heat. These factors restrict its utilization in applications that require comprehensive mechanical properties. This has therefore provided an impetus for significant theoretical and experimental research on the porosity formation and feeding efficiency of aluminum alloys.

Porosity manifests itself in various forms: massive shrinkage cavities, macroporosity, dispersed pores, or microporosity. Macroporosity results from solidification shrinkage that is not compensated by feeding of liquid metal. Generally, macroporosity occurs with short freezing range alloys. On the other hand, microporosity occurs in long freezing range alloys during dendritic solidification due to the failure of interdendritic feeding or due to the precipitation of hydrogen and other dissolved gases.[1]

Both theoretical and experimental studies have confirmed that local porosity in casting is related to the local thermal parameters.[2–7] Significant effort has been directed toward developing quantitative relationships between thermal parameter-based criteria functions and porosity formation during solidification of metals.[7–12] These relationships are also valid for long freezing range alloys.[13–21] Porosity criteria have been used in the computer simulation of solidification in casting to evaluate macroporosity in short freezing range alloys[8,9,19,22] and long freezing range alloys.[23–26] Some models based on the phenomenon of gas evolution during solidification were also developed to predict porosity formation.[27–30] A summary of various criterion functions developed to predict porosity formation has been given by Hansen and Sahm.[31–32]

Nomenclature	
B, B', C, M	constants
d_2	secondary dendrite arm spacing, μm
f_L	liquid fraction
$f_l(X)$	liquid fraction as function of distance in mushy zone, x
G	temperature gradient, °C/cm
K	permeability, cm^{-2}
L	casting length, m
l	length of the primary dendrite arm, m
l	length of interdendritic capillary, m
n	number of interdendritic channels per unit area, number/cm^2
R	radius cylinder casting, m
r	radius of liquid channel, m
t_f	solidification time, min
V_s	solidus velocity, cm/min
x	distance in mushy zone, m
β	solidification shrinkage
β'	$\beta/(1 - \beta)$
γ	parameter determined by dendritic structure
ΔP	pressure drop, Pa
ΔT	temperature range of solidification, °C
λ	heat flow constant
τ	tortuosity factor
ε:	cooling rate, °C/min
μ:	viscosity of flow, m · s

Qiming Chen and **C. Ravindran,** Centre for Near-Net-Shape Casting, Department of Mechanical Engineering, Ryerson Polytechnic University, Toronto, ON, Canada, M5B 2K3.

Although there is an extensive research literature on feeding and porosity formation in open mold cavity castings, literature for lost foam casting (LFC) is indeed limited. Recently, a preliminary study was carried out on the effect of feeding and thermal conditions on the soundness of a thin bar with lost foam process.[33] However, further research with a systematic design of casting under the condition of controlled hydrogen content in melt and constant static pressure is necessary. Thus, in this paper, a series of plate LFCs with controlled hydrogen content and various designs of feeder and gate were analyzed with thermal data and measurement of density distribution. For the casting with low hydrogen content, the interdendritic feeding mechanism is found to be predominant. With an increase of hydrogen content in the casting, the effect of gas pore growth becomes pronounced. With due consideration to these facts, there is a need to evaluate the effects of the basic thermal parameters and various criteria functions such as temperature gradient, G, local solidification time, t_f, solidus velocity, V_s, *Niyama*,[9] *LCC*,[11], and *KCL*[12] criterion functions on the porosity formation of A356 Al-Si-Mg alloys with lost foam process.

2. Theoretical Background

Campbell[1] has suggested four possible feeding mechanisms: liquid, mass, interdendritic, and solid feeding. Porosity results from the limitation of these feeding mechanisms. Interdendritic flow and evolution of gas pore during solidification are considered to be main causes for the formation of microporosity defects, because feeding mechanisms are operative at the low solid fraction.

Usually, the models of interdendritic feeding are derived from basic conservation relations, such as balances of thermal, mass, and momentum, and simplified by some assumptions from the mechanism of solidification that are solved by analytical and numerical methods.[25] Assuming a steady state, they can be derived directly from Darcy law in the mushy zone. The porosity predictions using theoretical parameters (criterion function such as *Niyama*, *LCC*, or *KCL*) of interdendritic feeding are consistent with those from empirical models (*FI* or *FEF*).[9,11,12]

The gas and porosity evolution model is derived using the mechanism of precipitation of gas during solidification.[27–30] The nucleation of porosity is considered from the surface tension and a critical value of the radius of pore nuclei, which is related to feeding behavior in the mushy zone. After nucleation of porosity, the gas precipitates and diffuses into the pore, resulting in the growth of porosity during solidification, assuming gas precipitation obeys Scheil law. However, in this study, only interdendritic feeding based on Darcy law is considered.

For theoretical considerations, a partially solidified long freezing range alloy is considered as a porous material. Piwonka and Flemings[5] assumed the flow with viscosity, μ, to take place in n channels per unit area. They assumed the effective channel length as casting length, L, multiplied by a tortuosity factor, τ. Based on the derivation by Walther *et al.*,[4] they gave:

$$\Delta P = \frac{32\mu\beta\lambda^2 L^2}{r^4}\left(\frac{\tau^2}{\pi R^2 n}\right) \qquad \text{(Eq 1)}$$

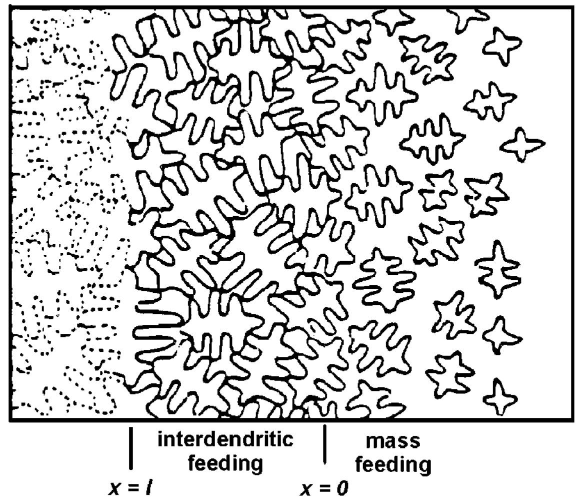

Fig. 1 Interdendritic feeding for equiaxial structure[11]

in which the net momentum change is neglected because of an assumption of steady-state flow velocity in the interdendritic channel.

Niyama *et al.*[9] applied Darcy's law to interdendritic flow and assumed that pressure in the liquid is atmospheric at a certain point in the interdendritic channel and decreases toward the end of the channel (root of dendrite):

$$\Delta P = \frac{\mu f_L \beta' Vs}{K}\int_0^{l_c} dx = \frac{\mu f_L \beta' Vs}{K} l \qquad \text{(Eq 2)}$$

The temperature gradient is defined as

$$G = \frac{\Delta T}{l} \qquad \text{(Eq 3)}$$

Thus,

$$\Delta P = \frac{\mu f \beta' \Delta T}{K}\frac{V_s}{G} \qquad \text{(Eq 4)}$$

The term V_s can be replaced with the cooling rate, ε, using the relationship

$$\varepsilon = V_s \cdot G \qquad \text{(Eq 5)}$$

Then,

$$\Delta P = \frac{\mu f \beta' \Delta T}{K}\frac{\varepsilon}{G^2} = M\frac{\varepsilon}{G^2} \qquad \text{(Eq 6)}$$

where M is a constant. The significance of Eq 6 is that material variables and thermal variables affecting pressure drop can be separated as a first-order approximation and the latter can be summed up in the form $G/\sqrt{\varepsilon}$.

Niyama *et al.*[9] employed the parameter $G/\sqrt{\varepsilon}$ to predict the formation of shrinkage porosity in cylindrical steel sand

Table 1 Casting design

Casting number	Gate size (cm) length × width × thickness	Feeder size (cm) length × width × thickness	Notes
P2-0f-2g(a)	2 × 3 × 2	...	sprue size (cm): 19 × 3 × 2.5
P2-5f-2g	2 × 3 × 2	5 × 5 × 7	...
P2-7f-2g	2 × 3 × 2	7 × 7 × 9	...
P2-0f-4g	4 × 3 × 2	...	sprue size (cm): 19 × 3 × 2.5

(a) P2-xf-xg: (plate thickness)-(feeder size)-(ingate length)

Table 2 Freezing ratio and volume ratio

Casting number	M_f (modulus of feeder, cm)	M_c (modulus of casting, cm)	FR (freezing ratio, M_f/M_c)	VR (volume ratio, V_f/V_c)	Soundness
P2-0f-2g	0.631579	0.470588	1.342105	0.125	unsound
P2-5f-2g	0.921053	0.470588	1.957237	0.455729	sound
P2-7f-2g	1.26	0.470588	2.6775	1.148438	sound
P2-0f-4g	0.631579	0.470588	1.342105	0.125	unsound

castings. Simultaneously, a finite difference heat-transfer program was used to calculate temperatures during solidification. A comparison of theoretical and experimental results showed the critical thermal gradient required to feed shrinkage to be inversely proportional to the diameter of castings. The parameter $G/\sqrt{\varepsilon}$ was proposed to be independent of the size and shape of the castings. A dimensional analysis by Hansen and Sahm[32] also confirmed this point.

Lecomte-Beckers[10] considered the fluid flow in the mushy zone in unidirectional solidification. With

$$K = \gamma f_L^2 \qquad \text{(Eq 7)}$$

$$\gamma = \frac{1}{24\pi n\tau^3} \qquad \text{(Eq 8)}$$

The local pressure drop at location x is given by

$$\Delta P = -\frac{\mu\beta' V_s}{\gamma}\int_0^x \frac{dx}{f_l(x)} \qquad \text{(Eq 9)}$$

The liquid fraction, $f_l\,(x)$, can be approximated by a linear law in the mushy zone:

$$f_l(x) = 1 - \left(\frac{x}{l}\right) \qquad \text{(Eq 10)}$$

where l is the length of the interdendritic capillary. Thus, Eq 9 becomes

$$\Delta P = \frac{l\mu\beta' V_s}{\gamma} \ln\frac{l}{l - x} \qquad \text{(Eq 11)}$$

Lee *et al.*[11] developed the model further for interdendritic feeding for equiaxial structure. Based on the feeding mechanics by Campbell,[1] the burst feeding for equiaxial structure includes mass feeding and interdendritic feeding, as shown in Fig. 1. However, there is a divergent point at $x = l$. For this reason, a characteristics length $x = l^* < l$ is introduced to circumvent a mathematical and physical singularity. Thus, Eq 11 becomes

$$\Delta P = \frac{l\mu\beta' V_s}{\gamma} \ln\frac{l}{l - l^*} \qquad \text{(Eq 12)}$$

The mushy zone length, l, can be expressed by Eq 3. With a generally accepted expression of γ as described in Eq 8 in which n is the number of interdendritic channels per unit area, which is inversely proportional to the square of secondary dendrite arm spacing (d_2), and

$$d_2 = Ct_f^{1/3} \qquad \text{(Eq 13)}$$

where C is a constant depending on the alloy, Lee *et al.*[11] gave

$$\Delta P = B\,\frac{V_s}{Gt_f^{2/3}} \ln\frac{l}{l - l^*} \qquad \text{(Eq 14)}$$

where $B = 24\pi\tau^3 C^2\ \mu\beta\Delta T$.

Kao *et al.*[12] considered that at the end of solidification, the solidification time, t_f, can be represented by

$$t_f = \frac{\Delta T}{GV_s} \qquad \text{(Eq 15)}$$

Thus, Eq 14 becomes

$$\Delta P = B'\,\frac{V_s^{1.6}}{G^{0.4}} \ln\frac{l}{l - l^*} \qquad \text{(Eq 16)}$$

where $B' = 24\ \pi\ \mu\beta\Delta T^{0.4}/C^2$.

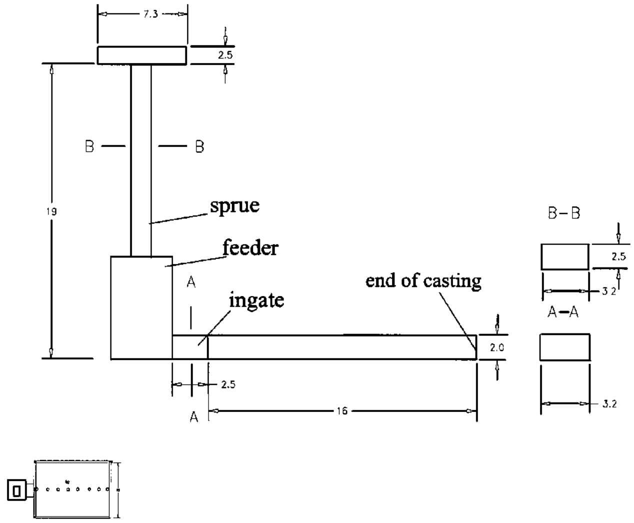

Fig. 2 An analysis of Caine's[17] type for the design of casting system

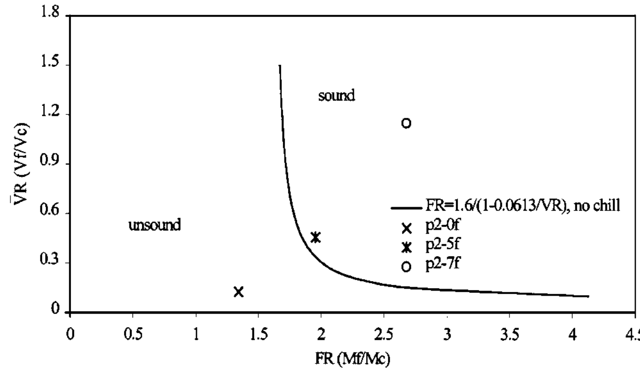

Fig. 3 Foam pattern design for the plate casting with dimensions in centimeters

The terms $LCC = Gt^{2/3}/V_s$ and $KCL = G^{0.4}/V_s^{1.6}$, in Eq 14 and 16 are used as the criterion functions to predict the porosity formation of aluminum alloys and are found to be validated by experimental results under the condition of very low hydrogen content.[11]

In summary, it can be seen that the criterion function with theoretical judgment is deduced from Darcy law, which evaluates the pressure drop introduced by interdendritic flow. When the pressure drop is high enough, shrinkage porosity results. Hence, these criterion functions apply to the aluminum alloys only with low hydrogen content, where gas porosity can be ignored.

3. Experimental Procedure

The geometry and the design of the casting system are summarized in Table 1 and shown in Fig. 2. With the analysis of Caine's type[17] shown in Table 2 and Fig. 3, a set of plate castings of 2 and 16 cm in length was designed with various sizes of feeder and gate, which connected the plate casting to the feeder. The intent of this design is to study the effect of the design on the thermal parameters and soundness of castings.

The pattern was constructed from expanded polystyrene with a density of 1.6 lb/ft^3 and was coated by dipping it in refractory slurry followed by drying in a forced air oven at 60 °C overnight. The foam pattern for the feeder was hollow to avoid the effect of decomposition of feeder pattern on the solidification of the plate casting. In order to minimize the effect of backpressure of the gas released from the decomposition of the foam pattern on the filling flow of liquid metal,[34] small gas vents (0.5 mm in diameter) were punched on the surface of the whole foam patterns. Thermocouples were inserted into the middle of the thickness of the patterns. A data acquisition system was employed to log the temperature data of each thermocouple. The foam pattern was installed in unbonded round silica sand of AFS Grain Fineness Number 35. Compaction of sand was carried out at 0.4 to 0.6 G of horizontal vibration for 30 s.

The charge of A356 ingot was melted in a gas fire furnace. After the charge was melted in a crucible, it was covered by cover flux and heated to 775 to 785 °C to compensate for the temperature drop during the degassing treatment. Degassing was carried out by plunging a potassium chloride tablet (Asbury Degasser Number 755) to the bottom of the crucible. Special care was taken to choose a proper temperature to avoid violent convection of the melt but to keep production of small bubbles for effective degassing. After degassing, the melt was covered with flux and the temperature was increased to 785 °C to enable further natural degassing. The reduced pressure test (RPT) samples were taken after the cycles of heating and air cooling of the melt. The densities of the RPT samples were measured by Archimedes principle. Thus, the hydrogen content of the melt was determined by the relationship developed by Mulazimoglu *et al.*[35] When the hydrogen content dropped to a desired level, the melt was poured with an insulated sleeve on the top of the vertical sprue of the pattern. Pouring temperature was controlled at 765 to 775 °C with consideration to the endothermic effect of degradation of the lost foam pattern during mold filling. The hydrogen content of the castings is listed in Table 3.

The specimens were sectioned near the position of thermocouples for density measurement. The densities were determined by Archimedes principle. The density measurement was carried out using an electronic balance with an accuracy of 0.001 g. Maximum density of the A356 alloy was determined to be 2.685 g/cm^3. All the density measurements were repeated for confirmation.

4. Results and Discussion

In the lost foam process, the filling rate is controlled by the degradation rate of the foam pattern. This provides a filling condition without turbulent flow and minimizes airflow into the melt, using a properly designed casting system. In this research, the gas vents on the surface of the pattern and compacting sand facilitated the release of the products of degradation of the foam pattern into loose sand in a relatively short time, which minimized the chance of these products' influence on the soundness of the casting. An extensive thermal data analysis was carried out with the cooling curve and the first derivative of the cooling curve. The calculation of thermal parameters

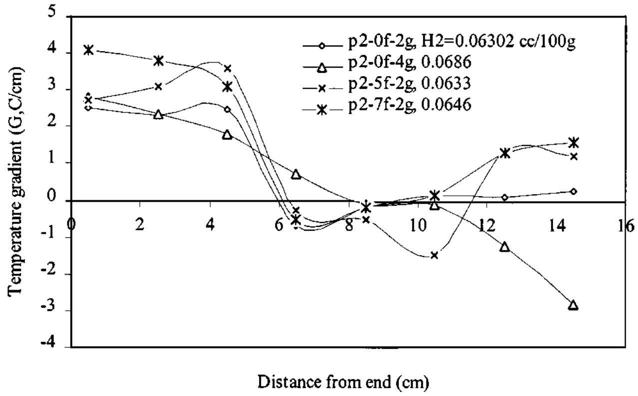

Fig. 4 Temperature gradient vs distance for plate castings

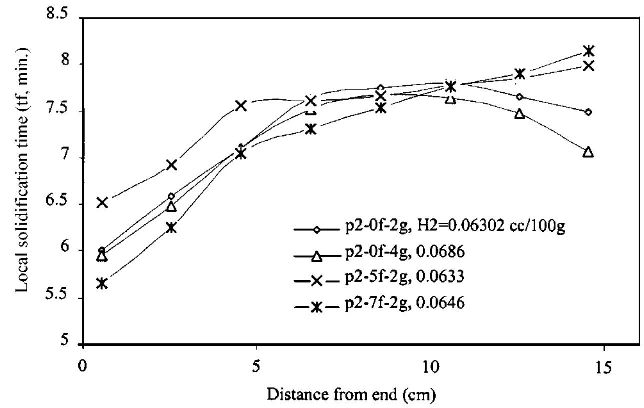

Fig. 6 Local solidification time vs distance for plate castings

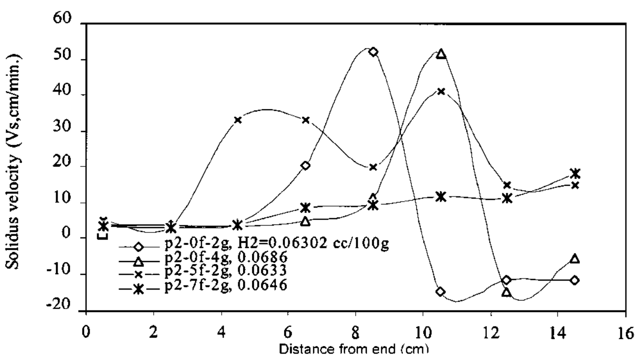

Fig. 5 Solidus velocity vs distance for plate castings

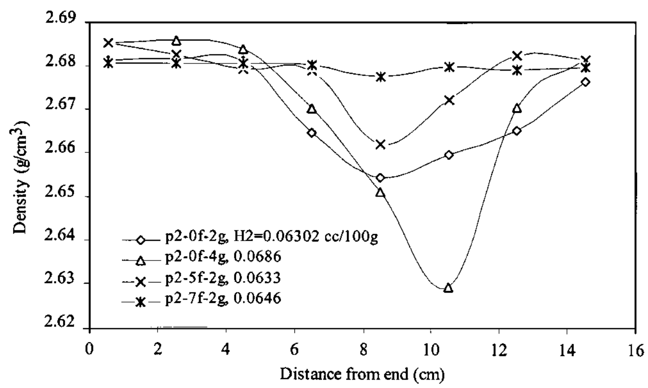

Fig. 7 Density distribution along the length of plate castings

Table 3 Hydrogen content of casting

Casting number	H_2 (cc/100 g)
P2-0f-2g	0.0630
P2-5f-2g	0.0633
P2-7f-2g	0.0646
P2-0f-4g	0.0686
P2-5f-2g-R	0.138
P2-0f-2g-R	0.248
P2-0f-3g	0.105

during solidification was described in detail in a previous study.[33]

Thermal conditions are characterized by temperature gradient G, local solidification time t_f, and solidus velocity V_s, which can be modified by various designs of feeders and gate size. They are shown in Fig. 4 to 6. The temperature gradient is highest at the end side of plate castings due to the edge effect of cooling. A lower temperature gradient can be seen at the feeder side of castings as the gate between the casting and feeder restricts feeding ability. However, the middle section of casting, "semi-infinite" area, shows the lowest value of temperature gradient. The larger feeder produces a higher temperature gradient, especially at the end side of the castings. For castings without a feeder, the positive value of temperature gradient at the end side changes to negative at the feeder or gate side; this suggests reversed directional solidification due to a cooling effect of the gate side. The hot spot at the middle of castings serves as the "feeder" to both sides of the plate casting, due to insufficient feeding at the feeder side of the casting. This also can be seen from local solidification time distributed along the length of casting. The positive continuous slope of local solidification time appears to characterize castings with a feeder. On the other hand, for the castings without a feeder, the local solidification time curve appears with positive and negative gradients at the end side and gate size, respectively. Since solidus velocity is equal to the reciprocal of gradient of local solidification time, the corresponding trend can be seen in Fig. 5. High solidus velocity corresponds to hot spot or semi-infinite area.

Feeding efficiency can be characterized by porosity or density level of the casting. The density distributions along the central line of the plate castings with low hydrogen content are shown in Fig. 7. In general, the highest density is found at the end side of the plate, where the fast cooling by the edge effect produced large temperature gradient and reduced solidus velocity. The density level along the length of the plate of casting depends on the feeder size and gate design as well as hydrogen content of the castings. A uniform distribution of porosity along the length of the casting can be obtained by using a larger feeder. Lower density appears at the semi-infinite area where neither edge effects of cooling nor feeding effects from the

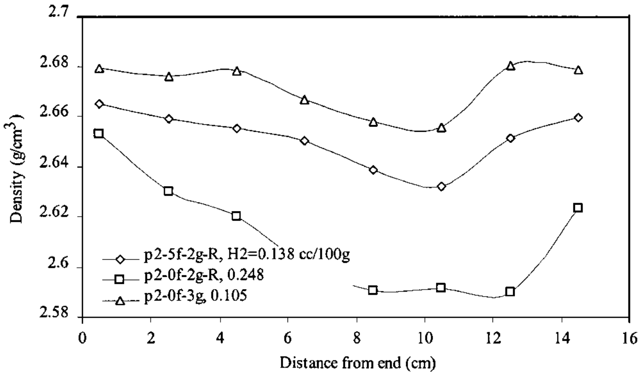

Fig. 8 Effect of hydrogen content on density of three castings with higher hydrogen content

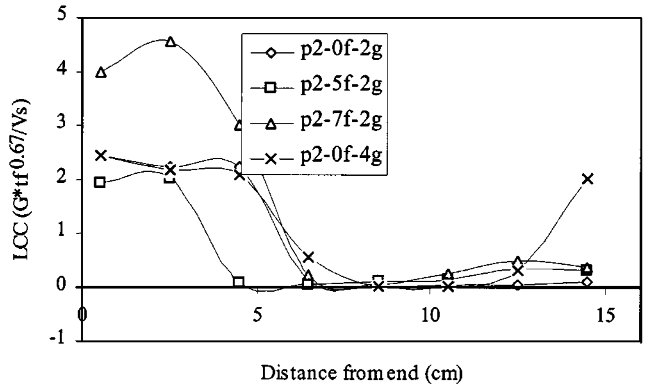

Fig. 11 Criterion function *LCC* vs distance end side of casting

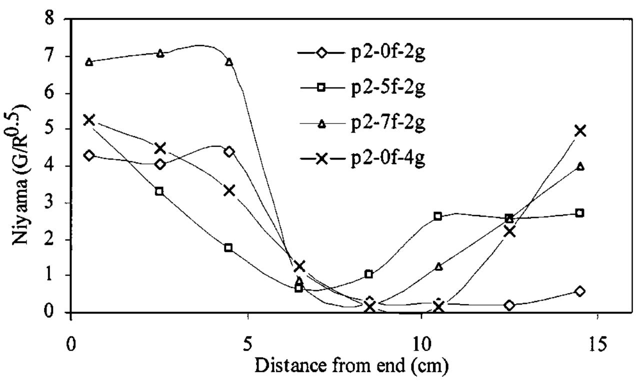

Fig. 9 Criterion function *Niyama* vs distance from end side of casting

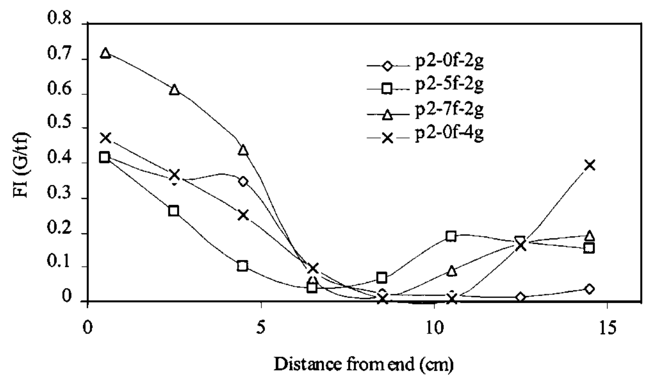

Fig. 12 Criterion function *FI* vs distance from end side of casting

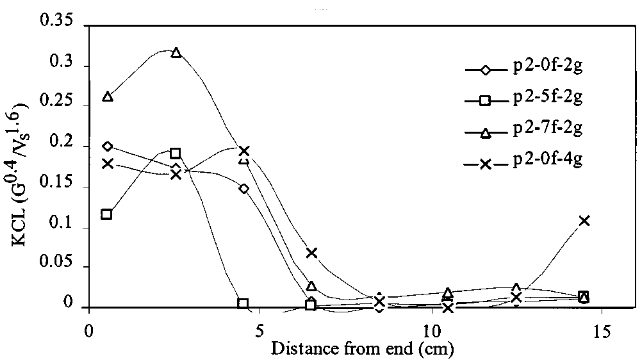

Fig. 10 Criterion function *KCL* vs distance from end side of casting

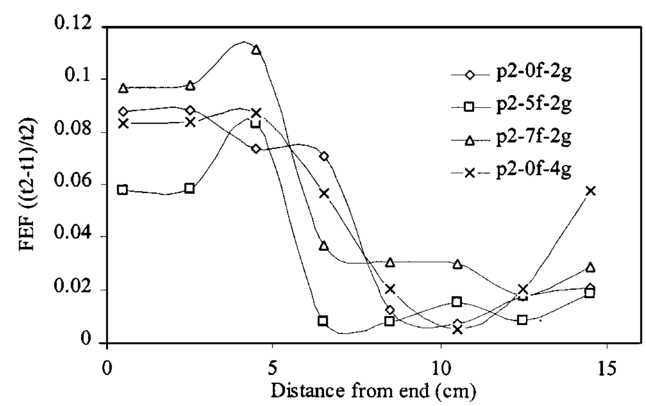

Fig. 13 Criterion function *FEF* vs distance from end side of casting

feeder are felt. The feeder gate restricted the feeding time for the feeder by solidifying ahead of the casting itself. The effect of hydrogen content on the density level is seen in Fig. 8. The lowest density level associates with high hydrogen content even when the casting is designed with a large feeder. Low hydrogen contents result in a high level of density distribution even without a feeder.

The criterion functions, *Niyama*, *LCC*, and *KCL*, are deduced from Darcy law; FI and FEF are empirical functions. All of these are calculated and plotted in Fig. 8 to 13 as functions of the distance from the end side. The distributions of these criterion functions based on Darcy law along the lengths of the castings shows high consistency with each other, which supports the interdendritic feeding mechanism, dominating over the 2 cm plate castings with lower hydrogen content. Microstructure analysis of the plate castings also confirms this point. For the samples with low hydrogen content, only shrinkage porosity appears in the form of the interdendritic net-work, as shown in Fig. 14, while for the samples with high hydrogen content, both shrinkage and gas pore were observed, which indicates

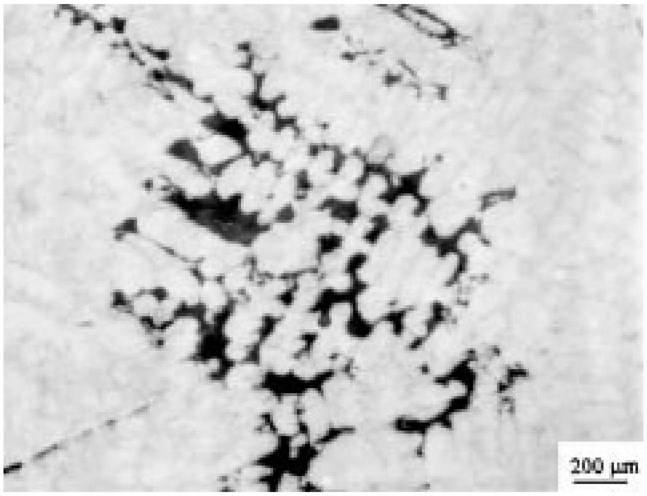

Fig. 14 Interdendritic shrinkage net work in plate casting (p2-0f-4g) with low hydrogen content (0.0686 cc/100g); magnification 50×

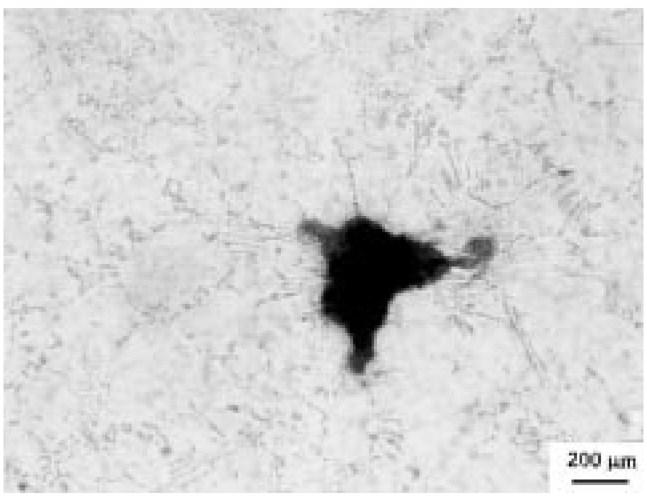

Fig. 15 Gas pore in plate casting (p2-0f-2gR) with high hydrogen content (0.248 cc/100 g) magnification 50×

that hydrogen influence is significant. A typical gas pore is shown in Fig. 15 for the plate casting with higher hydrogen content.

The temperature gradient is the most important thermal parameter of solidification to predict shrinkage formation with the interdendritic feeding mechanism. In Fig. 16, the temperature gradient is plotted against density distribution along the length of the castings. Large local temperature gradient decreases the feeding length at the micro-level and promotes progressive solidification on the macro-scale, thus decreasing the shrinkage porosity formation. A well-fitted trend line supports this hypothesis. Solidus velocity, V_s, has been plotted against density in Fig. 17. Despite some scatter in the data, a general trend of decrease in density with increase in solidus velocity is obvious. Since the solidus velocity is the reciprocal of the gradient of the local solidification time, it is a measurement of the tangent of the curve of local solidification time

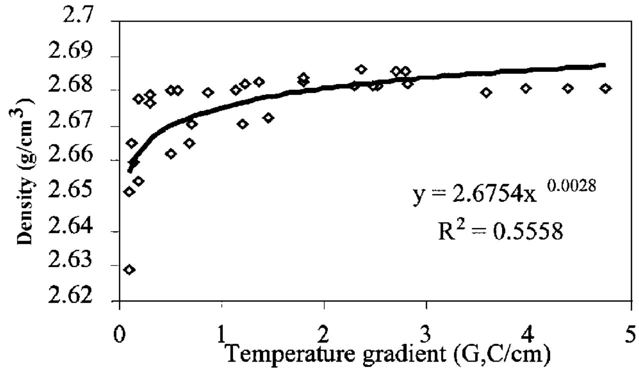

Fig. 16 Variation of density with temperature gradient (H_2 = 0.06 to 0.07 cc/100g)

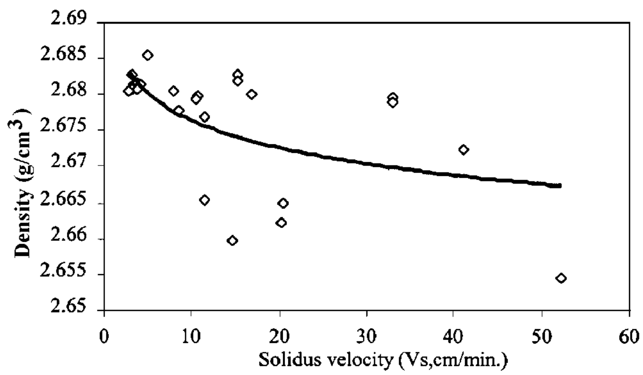

Fig. 17 Variation of density of solidus velocity (H_2 = 0.06 to 0.07 cc/100 g)

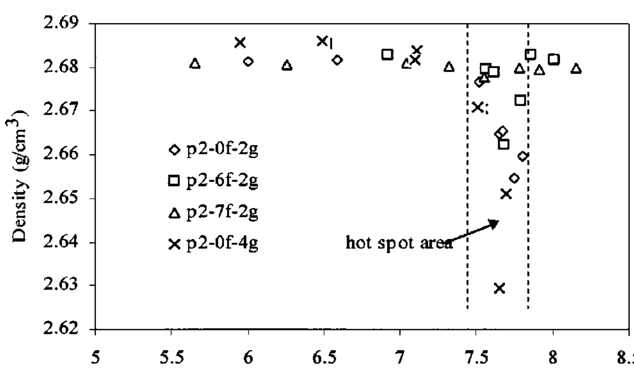

Fig. 18 Variation of density with local solidification (H_2 = 0.06 to 0.07 cc/100g)

versus the distance from the end of casting. Large V_s corresponds to the flat part of the curve near the reverse point or "hot spot" of casting, where the interdendritic feeding is poor. So it is not surprising to see a low density in the reverse point or hot spot area. Ignoring the density data in the hot spot area in Fig. 18 (since the density in this area drastically changed with a very small increment of the local solidification time, which indicates the poor feeding condition in the hot spot area), it can be seen that there is no effect of local solidification

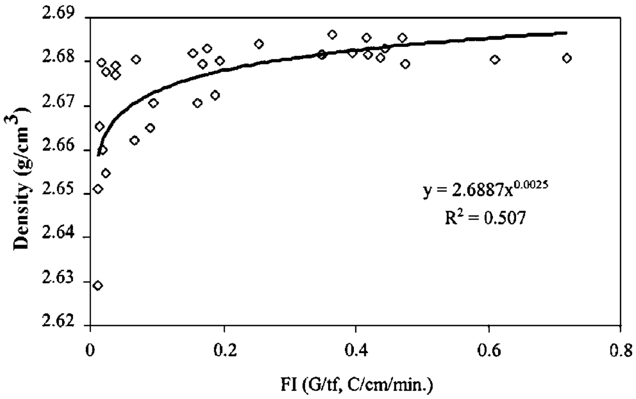

Fig. 19 Density as a function of *FI* (H_2 = 0.06 to 0.07 cc/100 g)

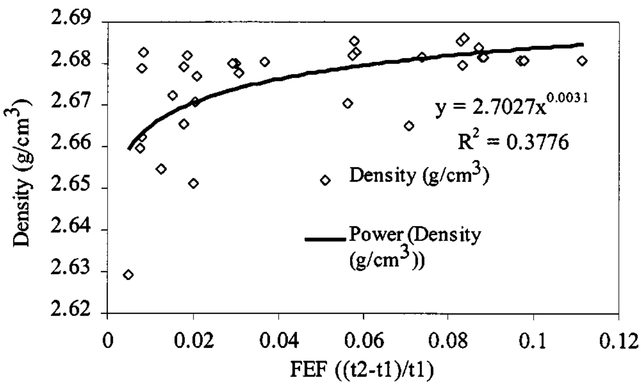

Fig. 20 Density as a function of feeding efficiency factor (H_2 = 0.06 to 0.07 cc/100 g)

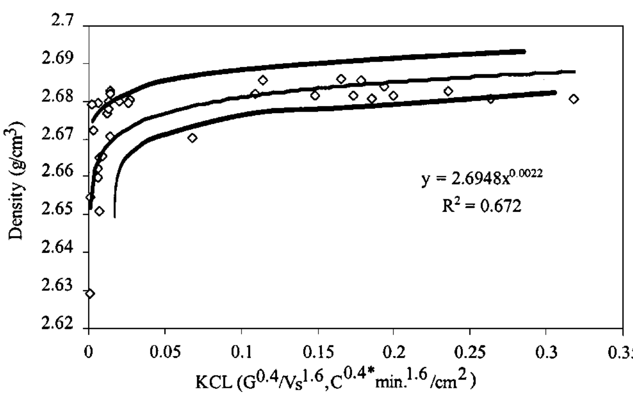

Fig. 21 Density as a function of *KCL* criterion function (H_2 = 0.06 to 0.07 cc/100 g)

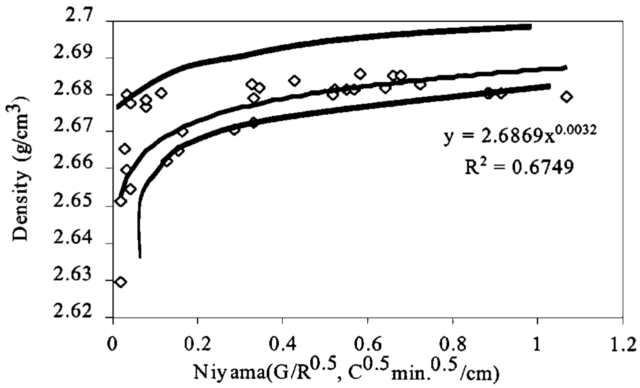

Fig. 22 Density as a function of *Niyama* criterion function (H_2 = 0.06 to 0.07 cc/100 g)

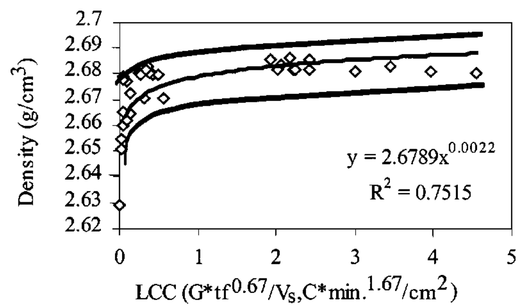

Fig. 23 Density as a function of *LCC* criterion function (H_2 = 0.06 to 0.07 cc/100 g)

time on the density distribution of the castings. This indirectly confirms that the interdendritic feeding prevailed in the solidification of the 2 cm thickness casting with low hydrogen content in the current research.

The correlation between porosity level and criterion function is shown in Fig. 19 to 23. The distribution related freezing index (*FI*) and freezing efficiency factor (*FEF*) to density are shown in Fig. 19 and 20. Better correlation can be obtained with a standard criterion function, such as *Niyama*, *LCC*, or *KCL* (Fig. 21 and 23). It is seen that the trend lines fit the experimental data well, which indicates that the thermal condition determines the formation of shrinkage under a given condition if the hydrogen content of the melt is low enough. Some dispersed data around the fitted line might be a result of error in measurement. The *Niyama* function has been found to be a geometry independent criterion function for steel alloys with short freezing temperature ranges.[9,32] However, for aluminum alloys, the *Niyama* function has been observed to be geometry dependent.[24] This controversy is attributed to the precipitation of hydrogen in aluminum alloys, which results in gas pore formation. The gas pore size will increase with an increase of local solidification time for high hydrogen content, as shown in Fig. 24. On the other hand, the local solidification time is a function of casting geometry or the modulus of the casting. As a result, the influence of local solidification time on the porosity formation is more significant, instead of *Niyama*, *LCC*, and *KCL* criterion functions, for aluminum alloy if the hydrogen content in the melt is high (Fig. 24 and 25). Since criterion functions such as *Niyama*, *LCC*, and *KCL* are derived from the interdendritic feeding mechanism with Darcy law, their application is limited to aluminum alloys with very low hydrogen content. However, the criterion functions can still be applied

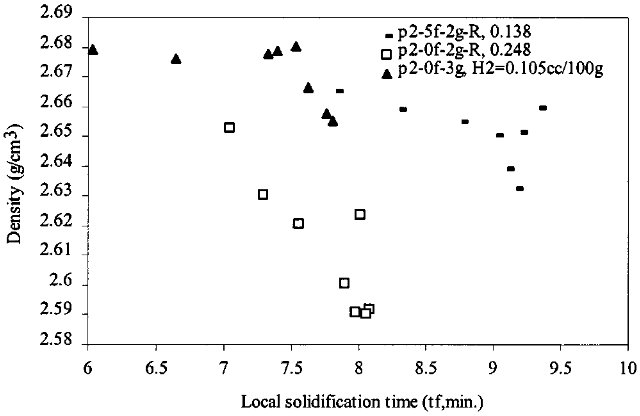

Fig. 24 Effect of local solidification time on density (H_2 = 0.10 to 0.25 cc/100 g)

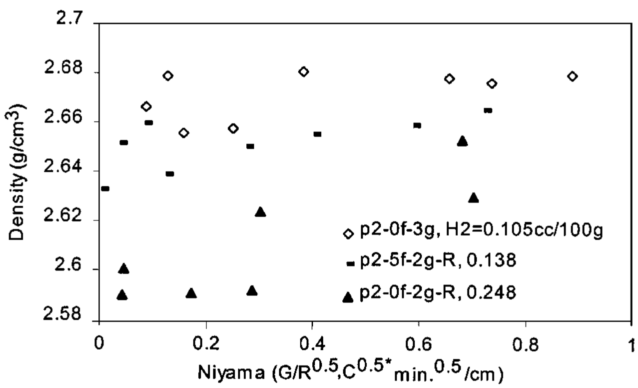

Fig. 25 Influence of hydrogen content on *Niyama* and density

to LFC of A356 Al-Si alloy to predict the shrinkage porosity formation with the restriction. For a casting with thickness of 2 cm, low hydrogen content of 0.06 to 0.07 cc/100 g and a good feeding condition will prevent the formation of the visible porosity in LFC. In the case of higher hydrogen content, the influence of gas (H_2) pore formation becomes predominant and cannot be ignored. Therefore, a criterion function that includes the effect of hydrogen content on the gas pore formation has been developed by the authors and will be published elsewhere.[36]

5. Conclusions

An analysis of literature on the feeding behavior of casting shows that the criterion functions to predict porosity formation are derived from Darcy law, which describes the relation of the pressure drop of feeding flow to the thermal parameters during solidification. For aluminum alloys, their application is limited to casting with low hydrogen content; thus, the gas pore formation from hydrogen content can be ignored.

A series of plate castings with lost foam process were cast to investigate the effect of feeding system design on the thermal parameters and porosity formation under the condition of low hydrogen content. Changing the design parameters of the feeding system strongly influences the thermal condition and the porosity formation of LFC. For hydrogen contents below 0.06 to 0.07 cc/100 g and 2 cm plate LFC, the interdendritic feeding prevails, which is confirmed by a well-fitted trend line to correlating density to the criterion functions derived from Darcy law, such as *Niyama*, *LCC*, and *KCL*. These criterion functions were applied to LFC under the experimental conditions. However, with increasing hydrogen content, the effect of local solidification time became pronounced. Further modeling of the effect of hydrogen content and local solidification time on the feeding efficiency of A356 alloy with the lost foam process is necessary as an extension of this research and will be published elsewhere.[36]

Acknowledgments

The authors thank F. Vinadolac for help with the experimental work. Financial support from the Natural Sciences and Engineering Research Council of Canada (NSERC) is acknowledged with gratitude.

References

1. J. Campbell: *AFS Cast Met. Res. J.*, 1969, Mar., pp. 1-8.
2. W.S. Pellini: *AFS Trans.*, 1953, vol. 61, pp. 61-80.
3. E.T. Myskowski, H.F. Bishop, and W.S. Pellini: *AFS Trans.*, 1953, vol. 61, pp. 302-08.
4. W.D. Walther, C.M. Adams, and H.F. Taylor: *AFS Trans.*, 1956, vol. 64, pp. 658-64.
5. T.S. Piwonka and M.C. Flemings: *Trans. TMS-AIME*, 1966, vol. 236, pp. 1157-65.
6. D. Apelian, M.C. Flemings, and R. Mehrabian: *Metall. Trans.*, 1974, vol. 5, pp. 2533-37.
7. N. Streat and F. Weinberg: *Metall. Trans. B*, 1976, vol. 7B, pp. 417-23.
8. V. de. L. Davies: *AFS Cast Met. Res. J.*, 1975, vol. 11, pp. 33-44.
9. E. Niyama, T. Uchida, M. Morikawa, and S. Saito: *AFS Int. Cast Met. J.*, 1981, June, pp. 16-22.
10. J. Lecomte-Beckers: *Metall. Trans. A*, 1988, vol. 19A, pp. 2341-48.
11. Y.W. Lee, E. Chang, and C.F. Chieu: *Metall. Trans. B*, 1990, vol. 21B, pp. 715-22.
12. S.T. Kao, E. Chang, and Y.W. Lee: *Mater. Trans. JIM*, 1994, vol. 35 pp. 632-39.
13. F.M. St. Johon, W. Wu, and J.T. Berry: *AFS Trans.*, 1968, vol. 76, pp. 645-54.
14. D.R. Irani, and V. Kondic: *AFS Trans.*, 1969, vol. 7, pp. 208-11.
15. J.T. Berry: *AFS Trans.*, 1970, vol. 78, pp. 421-28.
16. G.V. Kutumba Rao and, V. Panchanathan: *AFS Trans.*, 1973, vol. 81, 110-14.
17. E.N. Pan, C.S. Lin, and C.R. Loper, Jr.: *AFS Trans.*, 1990, vol. 98, pp. 735-46.
18. E.N. Pan, H.S. Chiou, and G.J. Liao: *AFS Trans.*, 1991, vol. 99, pp. 605-21.
19. S.T. Kao, and E. Chang: *AFS Trans.*, 1996, vol. 104, pp. 545-49.
20. S.T. Kao, E. Chang, and L.C. Chan: *AFS Trans.*, 1995, vol. 103, pp. 531-36.
21. S.T. Kao, E. Chang, and D. Hong: *AFS Trans.*, 1995, vol. 103, pp. 581-86.
22. S. Minakawa, I.V. Samarasekera, and F. Weinberg: *Metall. Trans. B*, 1985, vol. 16B, pp. 823-29.
23. I. Imafuku: *AFS Trans.*, 1983, vol. 91, pp. 527-40.
24. V. Laurent and C. Rigaut: *AFS Trans.*, 1992, vol. 100, pp. 647-55.
25. K. Kubo and R.D. Pehlke: *Metall. Trans. B*, 1985, vol. 16B, pp. 359-66.

26. H.F. Bishop, E.T. Myskowski, and W.S. Pellini: *AFS Trans.*, 1951, vol. 59, pp. 171-80.
27. D.R. Poirier, K. Yeum, A.L. Maple: *Metall. Trans. A*, 1987, vol. 18A, pp. 1979-87.
28. K. Yeum and D.R. Poirier: *Light Metals* 1988 TMS, Warrendale, PA, 1987, pp. 469-76.
29. J. Zou, S. Shivkumar, and D. Apelian: in *Materials Processing in the Computer Age*, V.R. Voller, M.S. Stachowicz, and B.G. Themas, eds., TMS, Warrendale, PA, 1991, pp. 389-401.
30. V.K. Suri and A. Paul: *AFS-Trans.*, 1993, vol. 101, pp. 949-54.
31. P.N. Hansen and P.R. Sahm: in *Modeling of Casting and Welding Processes IV*, A.F. Giamei and G.J., Abbaschian, eds., TMS, Warrendale, PA, 1988, pp. 33-42.
32. P.N. Hansen, P.R. Sahm, and E. Flender: *AFS Trans.*, 1993, vol. 101, pp. 443-46.
33. O. Chen and C. Ravindran: *Light Metals* 1999, Proc. 38th Annual Conf. of Metallurgists, Quebec City, PQ, Aug 22–26, 1999.
34. L. Wang, S. Shrivkumar, and D. Apelian: *AFS Trans.*, 1990, vol. 181, pp. 923-33.
35. M.H. Mulazimoglu, N. Handiak, and J.E. Gruzleski: *AFS Trans.*, 1989, vol. 180, pp. 225-32.
36. Q. Chen and Ravindran: *AFS Trans.*, 2000, accepted for publication.